Method for measuring the low-frequency sound power from a complex sound source based on sound-field correction in a non-anechoic tank

Hongzhe Xu(徐宏哲)[1,2,3], Qi Li(李琪)[1,2,3], Rui Tang(唐锐)[1,2,3,†], and Dajing Shang(尚大晶)[1,2,3]

[1] *Acoustic Science and Technology Laboratory, Harbin Engineering University, Harbin* 150001, *China*
[2] *Key Laboratory of Marine Information Acquisition and Security (Harbin Engineering University), Ministry of Industry and Information Technology, Harbin* 150001, *China*
[3] *College of Underwater Acoustic Engineering, Harbin Engineering University, Harbin* 150001, *China*

(Received 8 August 2022; revised manuscript received 1 December 2022; accepted manuscript online 31 January 2023)

Similar to air reverberation chambers, non-anechoic water tanks are important acoustic measurement devices that can be used to measure the sound power radiated from complex underwater sound sources using diffusion field theory. However, the problem of the poor applicability of low-frequency measurements in these tanks has not yet been solved. Therefore, we propose a low-frequency acoustic measurement method based on sound-field correction (SFC) in an enclosed space that effectively solves the problem of measuring the sound power from complex sound sources below the Schroeder cutoff frequency in a non-anechoic tank. Using normal mode theory, the transfer relationship between the mean-square sound pressure in an underwater enclosed space and the free-field sound power of the sound source is established, and this is regarded as a correction term for the sound field between this enclosed space and the free field. This correction term can be obtained based on previous measurements of a known sound source. This term can then be used to correct the mean-square sound pressure excited by any sound source to be tested in this enclosed space and equivalently obtain its free-field sound power. Experiments were carried out in a non-anechoic water tank (9.0 m × 3.1 m × 1.7 m) to confirm the validity of the SFC method. Through measurements with a spherical sound source (whose free-field radiation characteristics are known), the correction term of the sound field between this water tank and the free field was obtained. On this basis, the sound power radiated from a cylindrical shell model under the action of mechanical excitation was measured. The measurement results were found to have a maximum deviation of 2.9 dB from the free-field results. These results show that the SFC method has good applicability in the frequency band above the first-order resonant frequency in a non-anechoic tank. This greatly expands the potential low-frequency applications of non-anechoic tanks.

Keywords: non-anechoic tank, complex sound source, sound-field correction, low-frequency sound power

PACS: 43.30.+m, 43.58.+z **DOI:** 10.1088/1674-1056/acb75c

1. Introduction

The survival of covert underwater vehicles such as submarines and underwater drones can depend on their acoustic stealth performance. As such, controlling and reducing radiated noise is an important task in the optimal design of underwater vehicles. Low-frequency sound waves propagate over long distances due to their low attenuation in seawater. Control of the low-frequency sound and vibration characteristics of underwater structures is thus a subject that has received great attention, and accurate measurement and evaluation methods are required to establish how well these characteristics are controlled. Sound power is an important parameter that is used to describe the acoustic characteristics of a sound source, and this can directly characterize its radiation intensity. Accurately measuring the sound power radiated from complex sound sources such as underwater vehicles is an important technical way to test the effectiveness of vibration- and noise-reduction strategies.

Traditional measurement methods for low-frequency acoustic characteristics tend to be carried out in an external free field (such as a lake or ocean).[1–4] However, due to the influence of external test conditions, such as wind, waves, and water depth, the efficiency of these tests is low, their measurement repeatability is poor, and they are expensive. In contrast, measurements in non-anechoic water tanks provide a more efficient and cheaper means of understanding the acoustic characteristics of underwater sources. Blake and Maga[5] were the first to demonstrate through experiments that a non-anechoic water tank satisfies the diffuse-field conditions in the frequency band above the Schroeder cutoff frequency; they also demonstrated that the diffusion field theory commonly used in a reverberation chamber in air is also applicable to a non-anechoic water tank. On the basis of their research work, after decades of development, non-anechoic tanks have been widely used in many fields, including the calibration of underwater transducers,[6–8] measurement of the acoustic parameters of underwater acoustic materials,[9,10] and measurement of the sound power radiated from complex structures.[11–14]

The premise of using diffuse-field measurement methods in a non-anechoic water tank is that the modal density in the

†Corresponding author. E-mail: tangrui@hrbeu.edu.cn
© 2023 Chinese Physical Society and IOP Publishing Ltd

tank will be sufficiently high that the measurement of the reverberation time will have very good consistency. However, in the frequency band below the Schroeder cutoff frequency, the number of normal modes in the unit band is too small, and the interference effects of the sound field cannot be removed. In this case, there is large uncertainty bias in the measurement of the reverberation time, and this means that the commonly used diffuse-field measurement methods are no longer applicable.[15] In addition, the Schroeder cutoff frequency f_s is closely related to the tank volume V (the smaller the value of V, the higher the value of f_s). To date, because of practical limits on their size, the application of non-anechoic water tanks in the low-frequency domain has been greatly restricted.

Theoretically, the application conditions of the diffuse-field measurement methods at low frequency can be satisfied by increasing the volume of the tank. However, with increasing volume, the costs of constructing and using a non-anechoic tank will increase sharply. In contrast, if it were possible to establish new measurement methods applicable to the low-frequency domain (below the Schroeder cutoff frequency), this would be a highly cost-effective solution. In recent years, there have been many research studies seeking to achieve this aim.

Zhang *et al.*[16] proposed a hybrid experimental and numerical approach to predict the sound power radiated from a vibrating structure in a non-anechoic tank. Since this method requires very strict precision in the numerical model, the prediction accuracy is relatively low when it is applied to a complex structure. Barnard *et al.*[17] developed the supersonic intensity in reverberant environments (SIRE) measurement technique, which can only be used to measure the narrow-band sound power and directivity of the sound source. The SIRE method relies on a large number of underwater vector sensors to obtain the sound pressure and normal velocity at each position on the measurement surface, which leads to high measurement costs. Zhang *et al.*[18] proposed a low-frequency extension measuring technique, and they demonstrated through experiments that the low-frequency sound power radiated from a simple sound source can be accurately obtained using this technique in a non-anechoic tank. However, whether this technique is applicable to complex sound sources has not yet been studied.

Some researchers have proposed that one or a small number of hydrophones could be placed close to a target under test for direct measurements. For instance: in a laboratory water tank, Van de Loock *et al.*[19] measured the low-frequency underwater acoustic radiation of a stainless-steel tube excited by an impact hammer; Xu *et al.*[20] measured the radiated sound generated by a steady gas jet from a submerged horizontal nozzle; and Li *et al.*[21] measured the noise radiated from the nozzle of a liquid-filled pipeline system. However, this kind of measurement method is rather approximate because it does not take into account the extremely uneven sound-field distribution in the tank caused by normal-mode interference in the low-frequency range; thus, the corresponding measurement results can only be used for simple analysis of the radiation characteristics of the tested target but not for accurate evaluation of the sound power. Currently, in a non-anechoic water tank, below the Schroeder cutoff frequency, finding a way to accurately measure the sound power radiated from complex sound sources is still a bottleneck problem in practical engineering.

In this paper, we propose a low-frequency acoustic measurement method based on sound-field correction (SFC) in an enclosed space. This method allows accurate measurements of the sound power radiated from complex sound sources (including various underwater vibrating structures) below the Schroeder cutoff frequency in a non-anechoic tank. The remainder of this paper is organized as follows. Section 2 introduces the theoretical background of the SFC method. Section 3 describes the verification experiments, in which the sound power radiated from a cylindrical shell model under the action of mechanical excitation was measured using the SFC method in a rectangular non-anechoic water tank. Section 4 presents the results of experiments, along with some analysis. Finally, conclusions are given in Section 5.

2. Theory

2.1. Sound field in a non-anechoic water tank

The use of non-anechoic water tanks for making acoustic measurements can usually be abstracted as the problem of a sound field in an enclosed space. A theoretical analysis method for a sound field in an underwater enclosed space can be established using normal mode theory.[22] We consider a point sound source at position coordinate $\boldsymbol{r}_0$ and with volume velocity Q. The observation point is at position coordinate $\boldsymbol{r}$, and the velocity potential function $\varphi(\boldsymbol{r})$ of the sound field in the tank satisfies the Helmholtz equation

$$\nabla^2\varphi(\boldsymbol{r})+k^2\varphi(\boldsymbol{r})=-Q\delta(\boldsymbol{r}-\boldsymbol{r}_0), \tag{1}$$

where $\delta(\cdot)$ is the Dirac functional. Expanding $\varphi(\boldsymbol{r})$ and $\delta(\boldsymbol{r}-\boldsymbol{r}_0)$ in the form of normal modes and substituting these into Eq. (1), it can be obtained that

$$\varphi(\boldsymbol{r},\boldsymbol{r}_0)=-Q\sum_n\frac{\varphi_n(\boldsymbol{r})\varphi_n(\boldsymbol{r}_0)}{(k^2-k_n^2)V\Lambda_n}, \tag{2}$$

where V is the volume of the tank; $k=2\pi f/c_0$ is the driving wavenumber, which depends on the driving frequency f; c_0 is the speed of sound in water; $\varphi_n(\boldsymbol{r})$ and k_n are the eigenfunction and eigenvalue of the nth normal mode in the tank; and Λ_n denotes the orthogonality factor for each $\varphi_n(\boldsymbol{r})$

$$\Lambda_n=\frac{1}{V}\iiint_V|\varphi_n|^2\,\mathrm{d}v, \tag{3}$$

in which $\mathrm{d}v$ is the volume differential. Since acoustic energy will be partly absorbed by the tank wall and the water medium in a non-anechoic water tank, k_n should be complex-valued, and the velocity potential function $\varphi(\boldsymbol{r},\boldsymbol{r}_0)$ cannot be infinite, although the nth-order resonance is excited when $k=k_n$. According to Ref. [23], k_n can be expressed in the form

$$k_n=\frac{\omega_n}{c_0}+\mathrm{j}\frac{\delta_n}{c_0}, \tag{4}$$

where δ_n is a damping factor that can represent the absorption characteristics of the sound field, and j is the imaginary unit.

Neglecting the time variation $\mathrm{e}^{-\mathrm{j}\omega t}$, the sound pressure at the observation point $\boldsymbol{r}$, $p(\boldsymbol{r},\boldsymbol{r}_0)$, can be expressed by the velocity potential function $\varphi(\boldsymbol{r},\boldsymbol{r}_0)$

$$p(\boldsymbol{r},\boldsymbol{r}_0)=-\mathrm{j}\rho\omega\varphi(\boldsymbol{r},\boldsymbol{r}_0)=\mathrm{j}Q\rho\omega\sum_n\frac{\varphi_n(\boldsymbol{r})\varphi_n(\boldsymbol{r}_0)}{(k^2-k_n^2)V\Lambda_n}, \tag{5}$$

where ρ is the density of water and $\omega=2\pi f$ is the driving angular frequency.

2.2. Significance of spatial averaging

According to Eq. (5), the square of the modulus of the sound pressure at observation point $\boldsymbol{r}$ in the water tank can be obtained as

$$|p(\boldsymbol{r},\boldsymbol{r}_0)|^2=(Q\rho\omega)^2\left[\sum_n\frac{|\varphi_n(\boldsymbol{r})|^2|\varphi_n(\boldsymbol{r}_0)|^2}{|k^2-k_n^2|^2V^2|\Lambda_n|^2}+\sum_{\substack{n\\ n\neq m}}\sum_m\frac{\varphi_n(\boldsymbol{r})\varphi_m^*(\boldsymbol{r})\varphi_n(\boldsymbol{r}_0)\varphi_m^*(\boldsymbol{r}_0)}{(k^2-k_n^2)(k^2-k_m^2)^*V^2\Lambda_n\Lambda_m^*}\right], \tag{6}$$

where $*$ denotes the complex conjugate. The first term in the square brackets $[\cdot]$ in Eq. (6) represents the incoherent superposition of the contributions of normal modes of each order to the sound energy at the observation point. The second term represents the superposition of different normal modes with interference between them. From the orthogonality of normal modes

$$\frac{1}{V}\iiint_V\varphi_n(\boldsymbol{r})\varphi_m^*(\boldsymbol{r})\,\mathrm{d}v=\begin{cases}0, & n\neq m,\\ \Lambda_n, & n=m,\end{cases} \tag{7}$$

and taking the spatial average of Eq. (6), the spatial average of the mean-square sound pressure in the tank is obtained as

$$\left\langle|p|^2\right\rangle=\frac{1}{V}\iiint_V|p(\boldsymbol{r},\boldsymbol{r}_0)|^2\,\mathrm{d}v=(Q\rho\omega)^2\sum_n\frac{|\varphi_n(\boldsymbol{r}_0)|^2}{|k^2-k_n^2|^2V^2\Lambda_n^*}, \tag{8}$$

in which the angular brackets $\langle\cdot\rangle$ denote the spatial average. Clearly, the second summation in Eq. (6) has been removed through the spatial averaging; that is, the effect of interference has been eliminated. Once the spatial average has been taken, the resulting mean-square sound pressure reflects the response of the sound field excited by the sound source emitting at a fixed position in the tank.

In Eq. (8), the term $|\varphi_n(\boldsymbol{r}_0)|$ is the amplitude of the nth-order normal mode at the location of the sound source, and the value of this will change if the sound source is moved. According to the expression of the normal modes (see Appendix A for details), taking mode (2,1,1) and mode (3,1,1) as examples, the waveforms of normal modes are shown in Fig. 1. Clearly, if the sound source is placed near a node of the nth-order normal mode, the value of $|\varphi_n(\boldsymbol{r}_0)|$ will approach zero; as a result, the nth-order normal mode will not be fully excited, even when $f=f_n$. In addition, the frequency intervals between adjacent normal modes in the low-frequency band are large (that is to say, there is no modal overlap); thus, in this case, there will not be an obvious resonance peak at f_n in $\langle|p|^2\rangle$. Consequently, $\langle|p|^2\rangle$ will not represent the true characteristics of the sound field in the water tank. However, if spatial averaging is also conducted for the sound source, then the impact caused by nodes can be eliminated, and the normal modes of each order in the tank (in the frequency range covered by the driving frequencies) will be fully excited. In this case, there will be an obvious resonance peak in $\langle|p|^2\rangle$ at each resonant frequency, and thus $\langle|p|^2\rangle$ will represent the true characteristics of the sound field in the water tank.

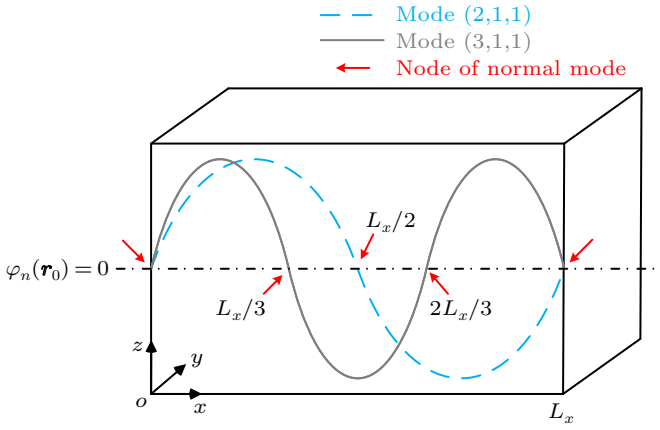


Fig. 1. Schematic diagram of waveforms along the x axis of mode (2,1,1) and mode (3,1,1) in a non-anechoic tank.

2.3. Basic principle of the SFC method

As shown in Fig. 2, there is a complex sound source in the non-anechoic water tank. The volume occupied by this sound source, which is much less than the tank's volume, is R, and the position coordinate of the center of this volume is $\boldsymbol{r}_0$. According to Ref. [24], a complex sound source can be viewed as a superposition of several independent simple sources, and the sound field excited by this complex source in an enclosed space is equivalent to a linear superposition of the sound fields excited by each independent simple source. Therefore, the complex sound source in the tank is equivalent to the superposition of M independent point sound sources in

volume R, and the sound pressure at the observation point $\boldsymbol{r}$ can be expressed as

$$p(\boldsymbol{r}) = \sum_{H=1}^{M} p(\boldsymbol{r}, \boldsymbol{r}_H) = \mathrm{j}\rho\omega \sum_{H=1}^{M} \sum_{n} \frac{Q_H \varphi_n(\boldsymbol{r}) \varphi_n(\boldsymbol{r}_H)}{(k^2 - k_n^2) V \Lambda_n}, \quad (9)$$

where Q_H and $\boldsymbol{r}_H$ $(H = 1, 2, \ldots, M)$ represent the volume velocity and position coordinate of the Hth point sound source, with $\boldsymbol{r}_H \in R$. At low frequency, since a small change in spatial position will make little difference to a normal mode, the values of $\varphi_n(\boldsymbol{r}_H)$ and $\varphi_n(\boldsymbol{r}_0)$ are thus almost the same; thus, Eq. (9) can be changed to

$$p(\boldsymbol{r}) = \mathrm{j}\rho\omega \sum_{H=1}^{M} Q_H \sum_{n} \frac{\varphi_n(\boldsymbol{r}) \varphi_n(\boldsymbol{r}_0)}{(k^2 - k_n^2) V \Lambda_n}. \quad (10)$$

Then, the spatial average of the mean-square sound pressure in the tank can be expressed as

$$\begin{aligned} \left\langle |p|^2 \right\rangle &= \frac{1}{V} \iiint_V |p(\boldsymbol{r})|^2 \, \mathrm{d}v \\ &= \rho^2 \omega^2 \left| \sum_{H=1}^{M} Q_H \right|^2 \sum_{n} \frac{|\varphi_n(\boldsymbol{r}_0)|^2}{|k^2 - k_n^2|^2 V^2 \Lambda_n^*}. \end{aligned} \quad (11)$$

To establish a relation between the sound field in the tank and the free field, the free-field sound power W of this complex sound source should also be expressed in the form of volume velocity. Now, if we can keep the position coordinates of this complex sound source unchanged while the non-anechoic water tank is replaced with a free field, then the sound pressure at position coordinate $\boldsymbol{r}'$ in far field can be expressed as[25]

$$p(\boldsymbol{r}') = -\mathrm{j}\omega\rho \sum_{H=1}^{M} \frac{Q_H \, \mathrm{e}^{\mathrm{j}k|\boldsymbol{r}' - \boldsymbol{r}_0|}}{4\pi |\boldsymbol{r}' - \boldsymbol{r}_0|}. \quad (12)$$

Since the sound intensity is $I = |p(\boldsymbol{r}')|^2 / 2\rho c_0$, W can be written as[26]

$$W = 4\pi \left| \boldsymbol{r}' - \boldsymbol{r}_0 \right|^2 I = \frac{\rho\omega^2}{8\pi c_0} \left| \sum_{H=1}^{M} Q_H \right|^2. \quad (13)$$

Using Eqs. (11) and (13), the ratio of the spatial average of the mean-square sound pressure in the non-anechoic tank to the free-field sound power of this complex sound source can be obtained as

$$\frac{\langle |p|^2 \rangle}{W} = 8\pi\rho c_0 \sum_{n} \frac{|\varphi_n(\boldsymbol{r}_0)|^2}{|k^2 - k_n^2|^2 V^2 \Lambda_n^*}. \quad (14)$$

In Eq. (14), the velocity potential function $\varphi_n(\boldsymbol{r}_0)$ is determined by the boundary conditions of the tank and the location of the sound source, the eigenvalue k_n is determined by the eigenfrequency of the tank, and the driving wavenumber k is determined by the driving frequency. Therefore, the value of $\langle |p|^2 \rangle / W$ is affected only by the acoustic properties of the tank, the location of the source, and the driving frequency; it is not affected by the characteristics of the source. That is, in a given non-anechoic water tank, the value of $\langle |p|^2 \rangle / W$ will be the same for different sound sources emitting at the same location under the same driving frequency, as long as the volumes of these sources are much less than that of the tank.

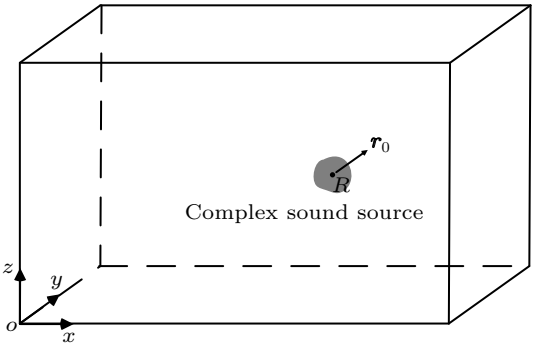


Fig. 2. Schematic diagram of a complex sound source in a non-anechoic water tank.

By multiplying both sides of Eq. (14) by $(1/p_{\mathrm{ref}}^2)/(1/W_{\mathrm{ref}})$ and expressing the result in logarithmic form, the transfer relationship between the spatial average sound pressure level SPL excited by the sound source in the tank and the free-field sound power level RPL of this sound source can be established:

$$\mathrm{SPL} - \mathrm{RPL} = \Delta\mathrm{corr}, \quad (15)$$

$$\mathrm{SPL} = 10\lg \frac{\langle |p|^2 \rangle}{p_{\mathrm{ref}}^2}, \quad (16)$$

$$\mathrm{RPL} = 10\lg \frac{W}{W_{\mathrm{ref}}}, \quad (17)$$

$$\Delta\mathrm{corr} = 10\lg \left[\frac{8\pi\rho c_0 W_{\mathrm{ref}}}{p_{\mathrm{ref}}^2} \sum_{n} \frac{|\varphi_n(\boldsymbol{r}_0)|^2}{|k^2 - k_n^2|^2 V^2 \Lambda_n^*} \right], \quad (18)$$

where p_{ref} and W_{ref} represent the reference sound pressure and the reference sound power, respectively, the values of which in water are generally $p_{\mathrm{ref}} = 1$ μPa and $W_{\mathrm{ref}} = 0.67 \times 10^{-18}$ W. By comparing Eqs. (14) and (18), it can be confirmed that Δcorr is affected only by the acoustic properties of the tank, the location of the source, and the driving frequency and not by the characteristics of the source. Therefore, Δcorr can be obtained based on previous measurements of a known sound source (meaning that the free-field sound power of this sound source is known) in the non-anechoic test tank, and Δcorr can be viewed as a fixed correction term. Using this correction term to correct the spatial average sound pressure level SPL excited by any sound source to be tested in this tank can equivalently obtain its free-field sound power level RPL:

$$\mathrm{SPL}^{\blacktriangle} - \mathrm{RPL}^{\blacktriangle} = \Delta\mathrm{corr}, \quad (19)$$

$$\mathrm{RPL} = \mathrm{SPL} - \Delta\mathrm{corr}. \quad (20)$$

In this work, the superscript ▲ is added to all physical quantities associated with the known sound source to distinguish

them from the corresponding physical quantities associated with the sound source to be tested. Equations (19) and (20) describe the basic principle of the SFC method.

3. Experiments

To verify the SFC method, experiments were carried out in a rectangular non-anechoic water tank (9.0 m × 3.1 m × 1.7 m) at the Underwater Acoustics Technology Lab of Harbin Engineering University, China. Since Eq. (15) is valid for any sound source with a volume much less than that of the tank, for convenience, an omnidirectional spherical sound source with a radius of 0.05 m [Fig. 3(a)] was used to obtain the correction term Δcorr for the sound field between this water tank and the free field. The free-field sound power level of the spherical sound source is known (see Appendix B for details). The thin-walled stainless-steel cylindrical shell model shown in Fig. 3(b) is the sound source to be tested; its axial length is 0.5 m, its radius is 0.25 m, its wall thickness is 0.003 m, and the thickness of the cover plates at each end is 0.014 m. During the experiments, a radial mechanical excitation force was applied to the shell at 0.14 m in the axial direction under the action of an internal longitudinal transducer to make the model vibrate. Additional weight was installed at the bottom of the model to overcome its buoyancy such that it would sink smoothly under the water.

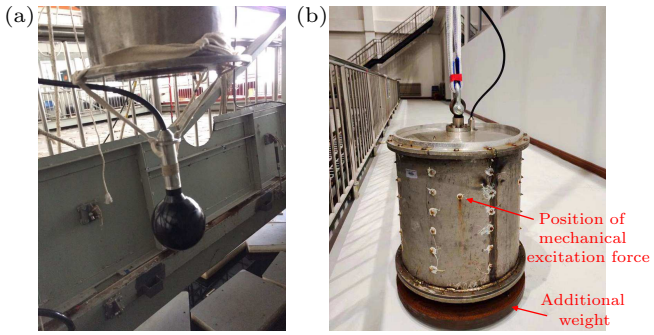


Fig. 3. (a) Spherical sound source. (b) Cylindrical shell model.

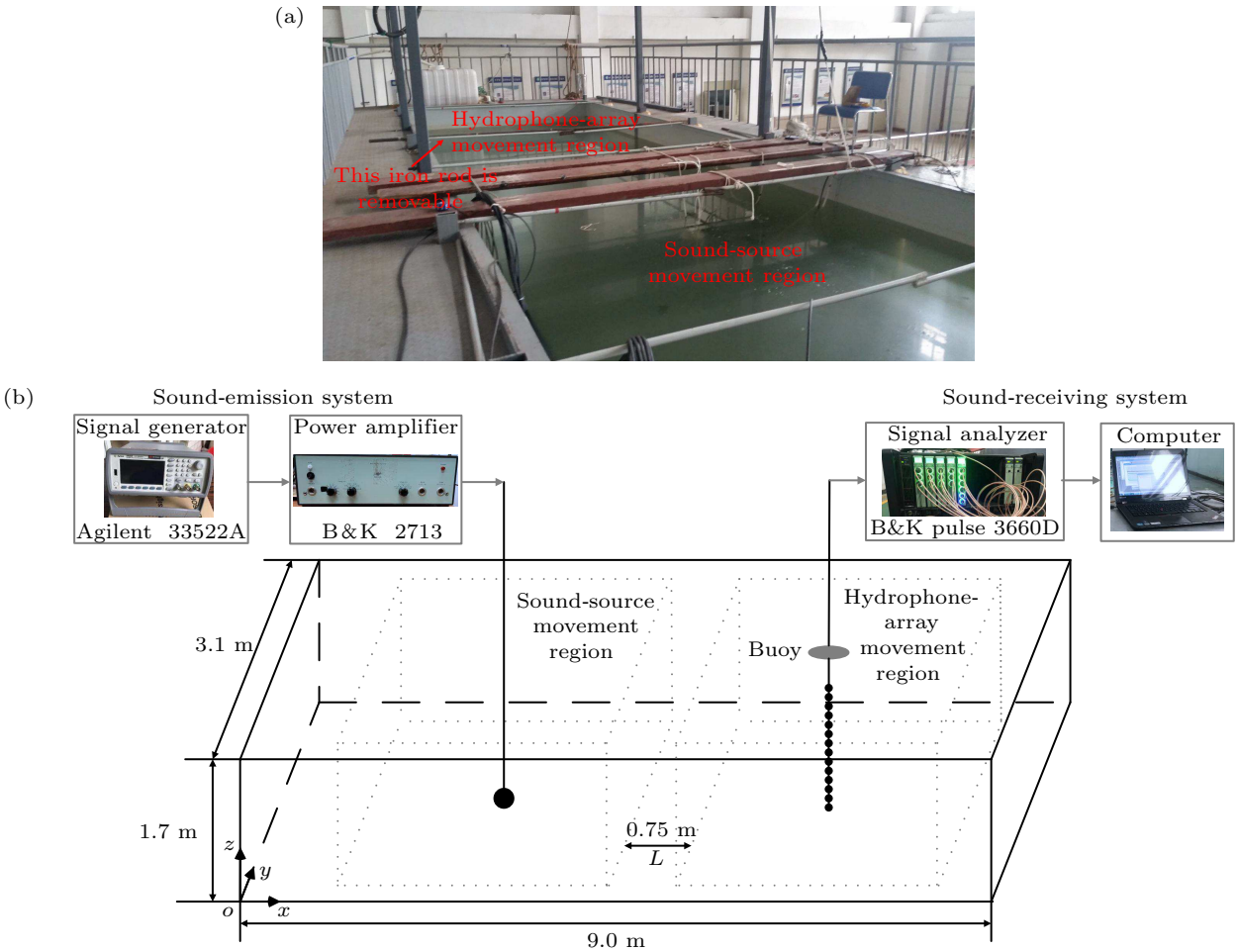


Fig. 4. (a) Photograph of the non-anechoic water tank. (b) Diagram of the system used for measuring the spatial average mean-square sound pressure excited by the spherical source.

The non-anechoic water tank [Fig. 4(a)] used in the experiments was made of iron; the water was allowed to settle in the tank for several weeks to eliminate any bubbles that might have caused scattering. The water temperature was 25 °C. The volume ratio of the tank to the cylindrical shell model was approximately 480:1; that is, the volume of the cylindrical shell model was much less than the volume of the tank. The experiments were divided into two parts. First, the spatial

average mean-square sound pressure excited by the spherical sound source was measured. Then, the spatial average mean-square sound pressure excited by the cylindrical shell model was measured.

3.1. Measuring the spatial average mean-square sound pressure excited by the spherical sound source

The measurement system is shown in Fig. 4(b). The hydrophone array consisted of 14 hydrophones (RHS-20, Hangzhou Applied Acoustics Research Institute; voltage sensitivity −198 dB re 1 V/μPa). The top hydrophone was 0.2 m away from the water surface, the bottom hydrophone was 0.2 m away from the bottom of the tank, and the distance between adjacent hydrophones was 0.1 m. The hydrophone array was suspended below a buoy, and it was driven to perform a spatial scanning movement by moving the buoy. A white-noise signal with an amplitude of 5.5 Vpp and a bandwidth of 0–3 kHz was generated by the signal generator (33522A, Agilent Technologies, Inc.) and amplified by the power amplifier (2713, Brüel & Kjær) at a fixed gain of 40 dB; this was then applied to the spherical sound source to make it emit stably. The spherical sound source could be made to perform a spatial scanning movement while emitting by moving a thin rope that was tightly connected to it.

Before the measurement began, we divided the non-anechoic tank into movement regions for the hydrophone array and for the sound source according to the following two requirements. (i) The minimum distance between the sound source and the hydrophone array must be at least twice the reverberation radius, i.e., $L \geq 2r_{\mathrm{c}}$ (where r_{c} is the reverberation radius, the value of which is determined as described in Ref. [27]). Thus, reverberation sound plays a major role in the hydrophone-array movement region and the contribution of direct sound can be ignored. (ii) When the hydrophone array and the spherical source perform spatial scanning movements simultaneously, the signal-to-noise ratio of the collected acoustic signal must not be less than 6 dB.

When the measurements began, the hydrophone array and the spherical source were slowly moved to perform spatial scanning in their respective regions simultaneously. During this period, the dynamic signal analyzer (PULSE 3660D, Brüel & Kjær) performed continuous data acquisition, and these data were stored in the computer after averaging 200 times. The movement of the hydrophone array and thus of the individual hydrophones meant that each sample from each hydrophone was equivalent to the mean-square sound pressure at a single fixed position in the tank; the measurement result of each hydrophone was the same as the average value of the mean-square sound pressure for the 200 fixed positions in the tank. Finally, the measurements from these 14 hydrophones were averaged to obtain the spatial average mean-square sound pressure of the sound field in the tank.

3.2. Measuring the spatial average mean-square sound pressure excited by the cylindrical shell model

Due to the limitations of the experimental conditions, the cylindrical shell model could only be used to emit in a fixed state, and it could not perform a spatial scanning movement while emitting like the spherical sound source. That is to say, spatial averaging could not be conducted for the cylindrical shell model directly. As an alternative, we measured the spatial average mean-square sound pressure $\langle |p_i|^2 \rangle$ excited by the cylindrical shell model when emitting at different positions (these emission positions were randomly selected in the sound source movement region, and they were asymmetrical). During the processing of experimental data, these $\langle |p_i|^2 \rangle$ values were averaged (see Subsection 4.2) so that spatial averaging for the cylindrical shell model could be achieved indirectly.

The measurement system is shown in Fig. 5. With the iron rod fixed onto the two wooden boards, moving them simultaneously along the length of the water tank can be used to adjust the position of the cylindrical shell model in the x direction; when the two wooden boards are fixed onto the water tank, moving the iron rod along the width of the tank can be used to adjust the position of the cylindrical shell model in the y direction. In addition, rotating the iron rod in the horizontal plane can drive the cylindrical shell model to perform circumferential rotation *in situ*; in this way, the direction of the excitation force from the internal longitudinal transducer can be changed without changing the position of the cylindrical shell model in the tank. The sound-receiving system used in these measurements was the same as that shown in Fig. 4(b), and all parameters and the movement region of the hydrophone array remained unchanged.

First, the cylindrical shell model was fixed at position 1 and it was rotated to align the direction of the excitation force with the $+x$ direction (denoted by $\boldsymbol{F}_x$ in Fig. 5). A white-noise signal with an amplitude of 0.3 Vpp and a bandwidth of 0–3 kHz was generated by the signal generator (33522A, Agilent), and this was amplified by the power amplifier (L6, Instruments, Inc.) at maximum gain and then applied to the longitudinal transducer inside the cylindrical shell model. This enabled the cylindrical shell model to vibrate under the excitation of the transducer. The spatial average mean-square sound pressure excited by the cylindrical shell model when emitting at position 1 was measured according to the sound-field acquisition and processing method described in Subsection 3.1. Next, with the excitation force continuing to point in the $+x$ direction, the cylindrical shell model was successively moved to positions 2 to 8 for emission and measurement. According to these steps, the spatial average mean-square sound pressures excited by the cylindrical shell model when emitting at each position were obtained. During all the measurements, the depth of the cylindrical shell model remained unchanged, and its upper end was 0.6 m away from the water surface.

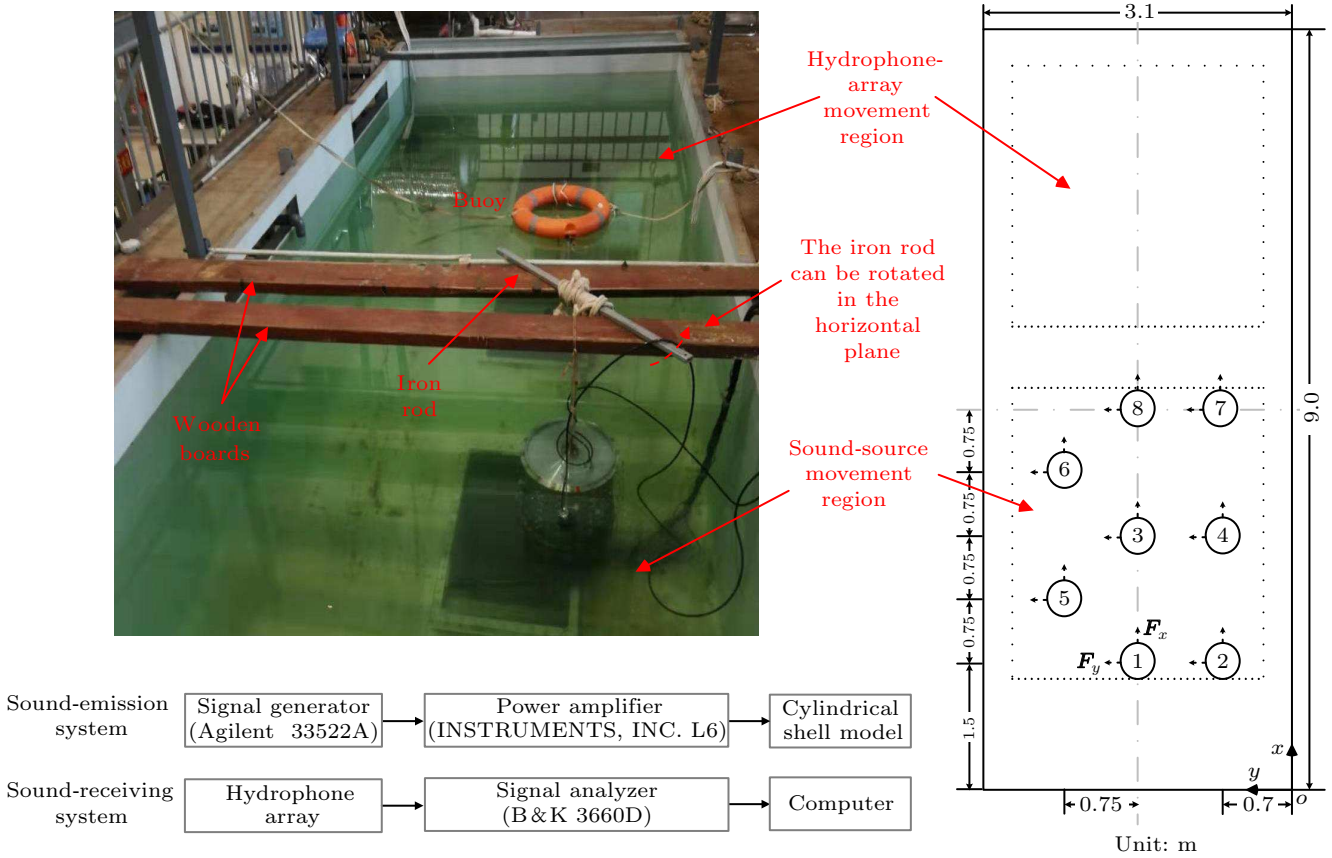


Fig. 5. Photograph and diagram of the system used for measuring the spatial average mean-square sound pressure excited by the cylindrical shell model.

To ensure that the results are not affected by the orientation of the excitation source, this was changed to point along the $+y$ direction (denoted by $\boldsymbol{F}_y$ in Fig. 5) by rotating the cylindrical shell model, and the spatial average mean-square sound pressures excited when emitting at positions 1 to 8 were again successively measured.

4. Results and analysis

4.1. Determining the frequency range for analysis

As described in Subsection 2.2, since spatial averaging has been conducted for the spherical sound source, the measured spatial average mean-square sound pressure can thus reflect the true characteristics of the sound field in the tank. This was plotted in the form of a sound pressure level [corresponding to $\mathrm{SPL}^{\blacktriangle}$ in Eq. (19)], as shown in Fig. 6.

It can be clearly distinguished from Fig. 6 that the first-order resonant frequency of the sound field in the tank is 480 Hz. In the frequency band below 480 Hz, there are no normal modes that can be excited in the sound field; the sound field thus has no response in this frequency range, and the SFC method cannot be used. In the frequency range 480 Hz–1120 Hz (in the 1/3-octave band, 1120 Hz is the upper-limit frequency corresponding to the center frequency of 1000 Hz), the resonance effect of the sound field is very strong, the modal density is relatively low, the frequency intervals of adjacent normal modes are relatively large, and the curve has strong fluctuations. In the frequency range 1120 Hz–2240 Hz (in the 1/3-octave band, 2240 Hz is the upper-limit frequency corresponding to the center frequency of 2000 Hz), as the frequency increases, the resonance effect of the sound field gradually decreases, the modal density gradually increases, modal overlap begins to appear, and the fluctuations of the curve gradually decrease. In the frequency band above 2240 Hz, the resonance effect of the sound field disappears, the modal density is high with strong modal overlap, and the curve is very smooth; on this basis, we can infer that this frequency is very close to the Schroder cutoff frequency.

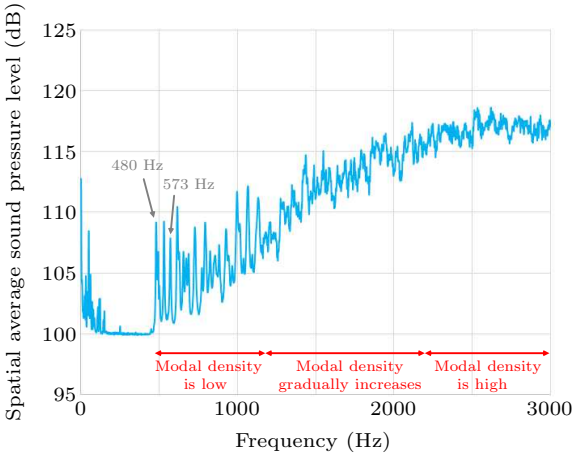


Fig. 6. Spatial average sound pressure level of the sound field in the non-anechoic tank.

In summary, 480 Hz–2240 Hz was selected as the frequency range for analysis in this work. In this frequency range, even if spatial averaging is used, the adverse effects of normal mode resonance on the sound field cannot be overcome. Next, the SFC method was used in this acoustic environment to obtain the free-field sound power of the cylindrical shell model.

4.2. Processing of the experimental data

Before the analysis, we present a brief description of the method that was used for processing the experimental data. Assuming that we now want to calculate the corresponding measurement results when the cylindrical shell model has D emission positions, the corresponding SPL can be obtained as

$$\mathrm{SPL} = 10\lg \frac{\left(\sum_{i}^{\boldsymbol{Z}} \langle |p_i|^2 \rangle\right)/D}{p_{\mathrm{ref}}^2}, \tag{21}$$

where $\langle |p_i|^2 \rangle$ denotes the spatial average mean-square sound pressure excited by the cylindrical shell model when emitting at position i ($i \in \boldsymbol{Z} \subset \{1,2,3,4,5,6,7,8\}$ and the number of i values is D). Then, combined with the relevant physical quantities $\mathrm{SPL}^{\blacktriangle}$ and $\mathrm{RPL}^{\blacktriangle}$ measured from the spherical source, the measurement results for the sound power level of the cylindrical shell model based on the SFC method can be obtained using Eqs. (19) and (20). First, the narrow-band measurement results are given, and then the measurement results in 1/3-octave bands are also given for the convenience of subsequent comparison and analysis.

According to the above description, all the experimental data corresponding to the direction of the excitation force being aligned with the $+x$ direction were processed first, and the obtained measurement results were divided into two categories for analysis, in which: (i) the cylindrical shell model had only a single emission position; (ii) the cylindrical shell model had multiple emission positions.

4.3. Measurement results when the cylindrical shell model had only a single emission position

Taking positions 5 and 8 as examples, the corresponding measurement results when the cylindrical shell model had only a single emission position were analyzed. Figure 7 shows the spatial average sound pressure level SPL excited by the cylindrical shell model when emitting at positions 5 and 8. As noted in Subsection 2.2, there is no guarantee that the normal modes of each order in the tank can be fully excited when the sound source is emitting at a single fixed position. In the frequency range 480 Hz–1120 Hz, due to the large frequency interval between the adjacent normal modes of the tank, if a normal mode of a certain order is not fully excited, this will have a serious impact on the sound field. For example, at $f = 573$ Hz (it can be determined from Fig. 6 that this frequency corresponds to a certain order normal mode of the tank), since this normal mode was not excited when the cylindrical shell model was emitting at position 8 but it was excited when emitting at position 5, this leads to the amplitude of the sound field when emitting at position 8 being much smaller than that when emitting at position 5. For this reason, there are obvious differences in the SPL values excited by the cylindrical shell model when emitting at different positions, and these SPLs cannot reflect the true characteristics of the sound field in the tank.

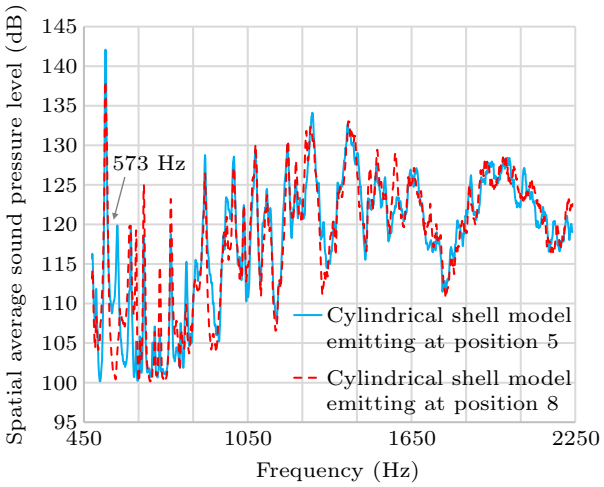


Fig. 7. Spatial average sound pressure levels excited by the cylindrical shell model when emitting at positions 5 and 8 (with $\boldsymbol{F}_x$ as the direction of the excitation force).

In the frequency range 1120 Hz–2240 Hz, due to modal overlap, even if a normal mode of a certain order is not fully excited, this will not have an obvious impact on the sound field. Therefore, the SPL values excited by the cylindrical shell model when emitting at different positions are similar and will largely reflect the true characteristics of the sound field in the tank.

Figure 8 shows the measurement results for the sound power level of the cylindrical shell model when emitting at position 5 in the non-anechoic tank, and figure 9 shows the corresponding results when emitting at position 8. In the frequency band 480 Hz–1120 Hz, because the spatial average sound pressure level excited by the cylindrical shell model when emitting at a single position cannot reflect the true characteristics of the sound field in the tank, the measurement results obtained using the SFC method in the non-anechoic tank have large deviations from the free-field results (see Appendix B for the process of obtaining the free-field results); the maximum deviations are 4.9 dB in Fig. 8(b) and 4.5 dB in Fig. 9(b). In the frequency band 1120 Hz–2240 Hz, since the spatial average sound pressure level excited by the cylindrical shell model when emitting at a single position can provide a good representation of the true characteristics of the sound field in the tank, the measurement results obtained using the SFC method in the non-anechoic tank are very close to the free-field results.

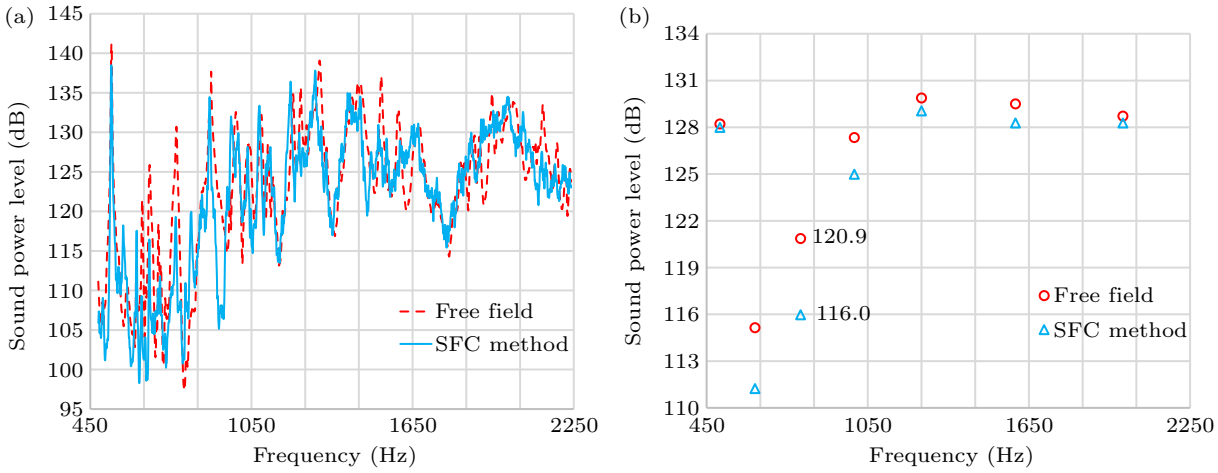


Fig. 8. Measurement results for the sound power level of the cylindrical shell model when emitting at position 5 (with $\boldsymbol{F}_x$ as the direction of the excitation force) (a) in narrow bands and (b) in 1/3-octave bands.

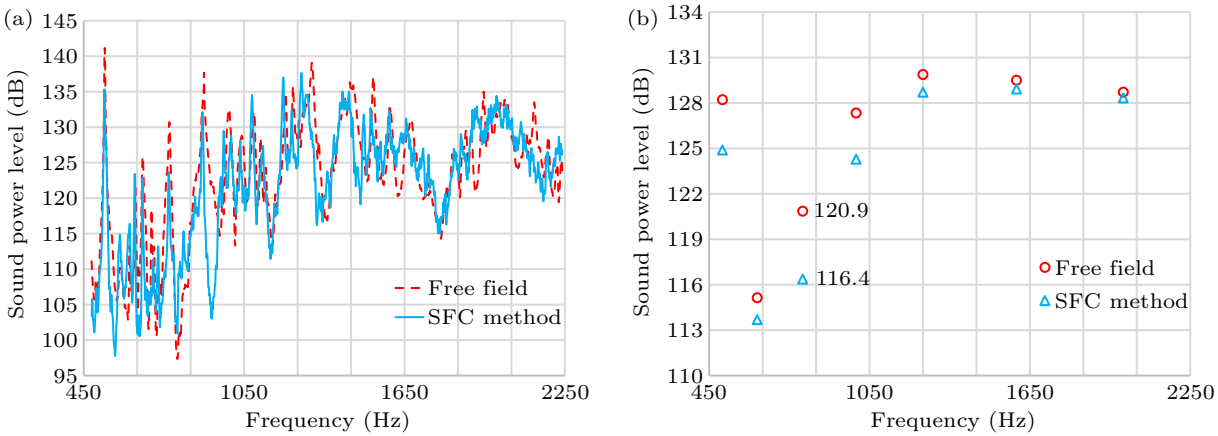


Fig. 9. Measurement results for sound power level of the cylindrical shell model when emitting at position 8 (with $\boldsymbol{F}_x$ as the direction of the excitation force) (a) in narrow bands and (b) in 1/3-octave bands.

4.4. Measurement results when the cylindrical shell model had multiple emission positions

Figure 10 shows the measurement results for the sound power level of the cylindrical shell model when four different emission positions were used [positions 5–8; that is, $\boldsymbol{Z} = \{5,6,7,8\}$ in Eq. (21)] in the non-anechoic tank. By comparing Figs. 10(b), 9(b), and 8(b), it can be seen that when the number of emission positions of the cylindrical shell model is increased from one to four, there is an obvious decrease in the measurement deviation of the SFC method in the frequency band 480 Hz–1120 Hz; the maximum deviation is reduced from 4.9 dB to 3.8 dB. This is because increasing the number of emission positions is equivalent to conducting spatial averaging for the cylindrical shell model, which helps to ensure that normal modes of all orders in the tank are fully excited, and the spatial average sound pressure level SPL can then better reflect the true characteristics of the sound field in the tank; the measurement deviation of the SFC method is thus reduced. In the frequency range 1120 Hz–2240 Hz, since the corresponding SPL value when using only a single emission position already reflects the true characteristics of the sound field in the tank well, increasing the number of emission positions has little effect on the measurement results obtained by the SFC method.

Continuing to increase the number of emission positions can come even closer to fully exciting the normal modes of each order in the water tank, and the spatial average sound pressure level SPL can thus even better reflect the true characteristics of the sound field in the tank. As a result, when the number of emission positions is increased from four to seven (Fig. 11), the maximum deviation of the SFC method is reduced from 3.8 dB to 3.0 dB; the sound power level of the cylindrical shell model measured in the non-anechoic tank using the SFC method then has a good consistency with the free-field results in the whole frequency band.

However, when the number of emission positions was increased from seven to eight (Fig. 12), the measurement results changed very little, and the maximum deviation of the SFC method only decreased by 0.1 dB (from 3.0 dB to 2.9 dB), indicating that using eight emission positions was sufficient for this experiment. In addition, the Δcorr values corresponding to the cylindrical shell model and the spherical sound source were calculated according to Eq. (15). For the convenience

of comparison and analysis, only the 1/3-octave spectrum of Δcorr is given in Fig. 12(c). As can be seen, the Δcorr values corresponding to the cylindrical shell model and the spherical sound source have good consistency, and the maximum deviation between them is 2.9 dB. This demonstrates that Δcorr is a fixed correction term for the sound field between this water tank and the free field, and it is not affected by the characteristics of the sound source.

All the experimental data corresponding to the direction of the excitation force being aligned with the $+y$ direction were also processed, and the obtained measurement results are presented in Appendix C. Similar conclusions can be drawn after analyzing these results, and these will not be repeated here. In summary, no matter the direction of the excitation force, the free-field sound power level of the cylindrical shell model can be accurately measured using the SFC method in the non-anechoic tank. This verifies the effectiveness of the SFC method.

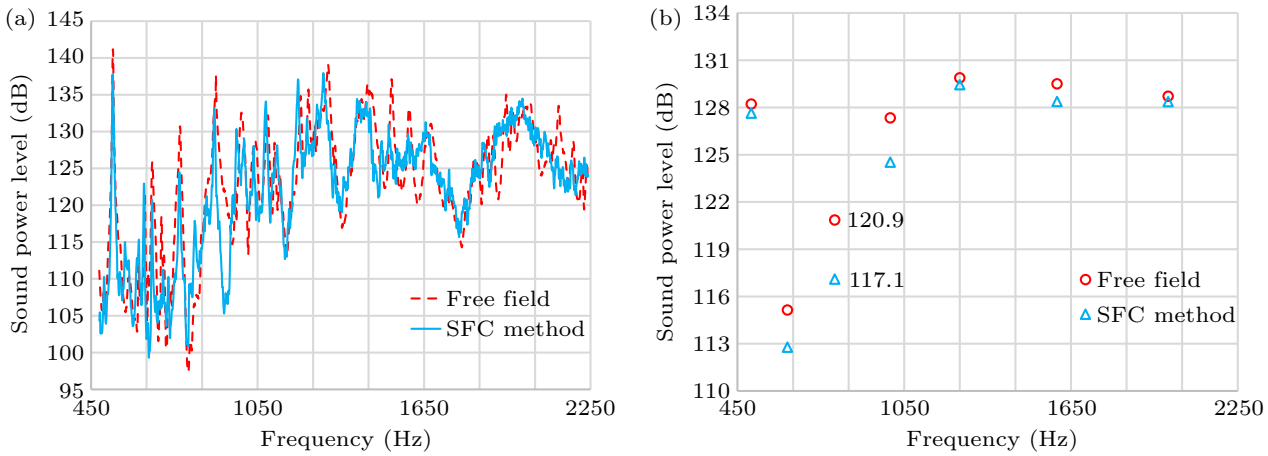


Fig. 10. Measurement results for the sound power level of the cylindrical shell model when four different emission positions were used (positions 5–8, with $\boldsymbol{F}_x$ as the direction of the excitation force) (a) in narrow bands and (b) in 1/3-octave bands.

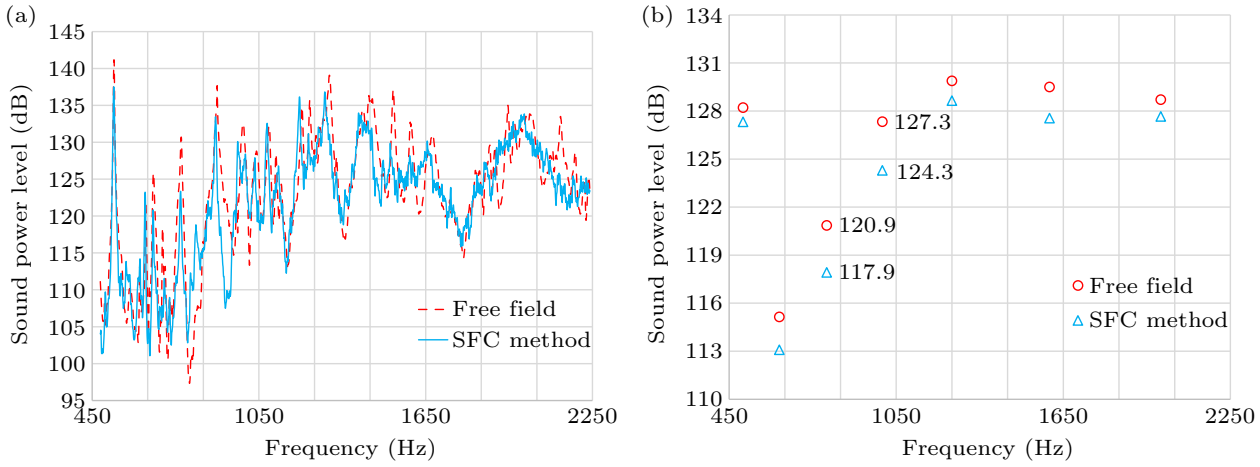


Fig. 11. Measurement results for the sound power level of the cylindrical shell model when seven different emission positions were used (positions 2–8, with $\boldsymbol{F}_x$ as the direction of the excitation force) (a) in narrow bands and (b) in 1/3-octave bands.

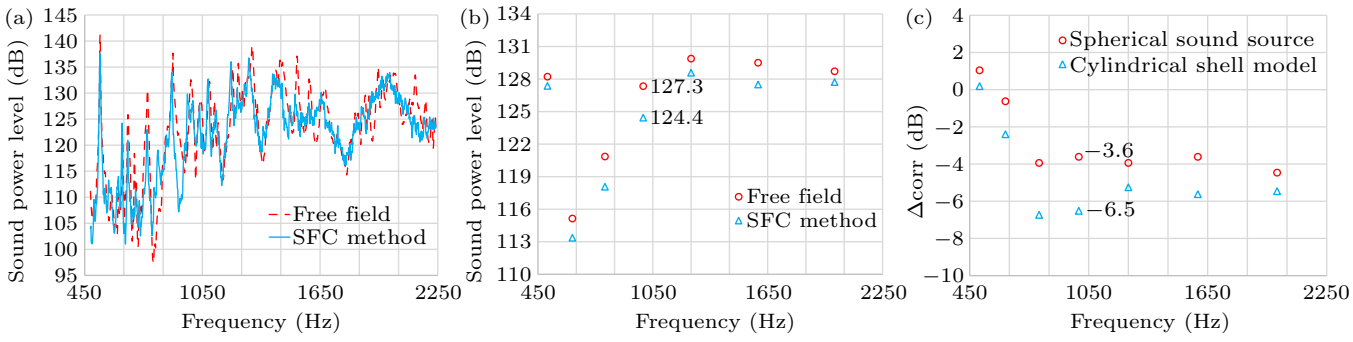


Fig. 12. Measurement results when using eight different emission positions (positions 1–8) for the cylindrical shell model (with $\boldsymbol{F}_x$ as the direction of the excitation force): (a) sound power levels of the model in narrow bands and (b) in 1/3-octave bands, and (c) 1/3-octave spectrum of Δcorr.

5. Conclusions

Herein, we propose a low-frequency acoustic measurement method based on sound-field correction in an enclosed space (the SFC method). This effectively solves the problem of measuring the sound power radiated from complex sound sources in the low-frequency band (below the Schroeder cutoff frequency) in a non-anechoic tank. In this method, based on normal mode theory, the transfer relationship between the mean-square sound pressure in an underwater enclosed space and the free-field sound power of the sound source is established, and this is regarded as a correction term for the sound field between this enclosed space and the free field. This correction term can be obtained based on previous measurements of a known sound source. Using this correction term to correct the mean-square sound pressure excited by any sound source to be tested in this enclosed space can equivalently obtain its free-field sound power. The sound power radiated from a cylindrical shell model under the action of mechanical excitation was measured using the SFC method in a non-anechoic water tank. The measurement results showed a maximum deviation of 2.9 dB from the free field results.

The results of this work show that when the volume of a sound source to be tested is much less than the volume of a non-anechoic tank in which it is tested, the SFC method has good applicability in the frequency band above the first-order resonant frequency. This greatly expands the potential low-frequency applications of non-anechoic tanks.

Appendix A: Normal modes in a rectangular non-anechoic water tank

Normal modes in a non-anechoic tank are analyzed here in a Cartesian coordinate system (x, y, z). The length, width, and depth of the rectangular non-anechoic tank used in the experiments are L_x, L_y, and L_z, and the thickness of the tank wall is negligible compared to L_x, L_y, and L_z. Since the whole tank is enveloped by air, the surface of the tank can be approximated as an absolute soft boundary.

In the absence of a sound source in the rectangular tank, the velocity potential function satisfies the homogeneous Helmholtz equation

$$\nabla^2\varphi + k^2\varphi = 0 \tag{A1}$$

with the boundary condition

$$\varphi|_{\Theta} = 0, \tag{A2}$$

where ∇^2 denotes the Laplacian operator; k is the acoustic wavenumber, which depends on the frequency of the sound field according to the relation $k = 2\pi f/c_0$; c_0 is the speed of sound in water; and Θ denotes the surface of the rectangular tank. The general solution satisfying Eqs. (A1) and (A2) can be obtained by separation of variables

$$\varphi_{n_x,n_y,n_z}(x,y,z) = \sin\left(\frac{n_x\pi}{L_x}x\right)\sin\left(\frac{n_y\pi}{L_y}y\right)\sin\left(\frac{n_z\pi}{L_z}z\right),$$
$$n_x, n_y, n_z = 1,2,3,\ldots \tag{A3}$$

The k^2 in Eq. (A1) can be replaced by k_n^2, which meets the eigenvalue conditions

$$k_n^2 = \left(\frac{n_x\pi}{L_x}\right)^2 + \left(\frac{n_y\pi}{L_y}\right)^2 + \left(\frac{n_z\pi}{L_z}\right)^2,$$
$$n_x, n_y, n_z = 1,2,3,\ldots, \tag{A4}$$

where k_n is the eigenvalue of the nth normal mode in the rectangular tank.

$$\varphi_n(x,y,z) = \varphi_{n_x,n_y,n_z}(x,y,z) \tag{A5}$$

and (n_x, n_y, n_z) denotes the mode number of the nth normal mode. The normal frequency (also called the resonant frequency) f_n in the rectangular non-anechoic tank is calculated using

$$f_n = \frac{c_0}{2\pi}k_n. \tag{A6}$$

From the orthogonality of normal modes

$$\frac{1}{V}\iiint_V \varphi_n\varphi_m \mathrm{d}v = \begin{cases} 0, & n \neq m, \\ \Lambda_n, & n = m, \end{cases} \tag{A7}$$

where V is the volume of the tank, and substitution of Eq. (A3) into Eq. (A7) gives $\Lambda_n = 1/8$.

According to Ref. [28], the total number of normal modes with a frequency lower than f in the rectangular tank is calculated using

$$N_f = \frac{4\pi}{3}V\left(\frac{f}{c_0}\right)^3 - \frac{\pi}{2}(L_xL_z + L_yL_z + L_xL_y)\left(\frac{f}{c_0}\right)^2 + \frac{L_x+L_y+L_z}{2}\frac{f}{c_0}. \tag{A8}$$

Thus, the number of normal modes in unit bandwidth around f, which we refer to as the modal density, is

$$\frac{\mathrm{d}N_f}{\mathrm{d}f} = \frac{4\pi}{c_0}V\left(\frac{f}{c_0}\right)^2 - \frac{\pi}{c_0}(L_xL_z + L_yL_z + L_xL_y)\frac{f}{c_0} + \frac{L_x+L_y+L_z}{2c_0}. \tag{A9}$$

Then, the Schroeder cutoff frequency f_s of the sound field in the rectangular tank can be obtained through the following equations:[29]

$$\left.\frac{\mathrm{d}N_f}{\mathrm{d}f}\right|_{f=f_s}\overline{\Delta f} \geq 3, \tag{A10}$$

$$\overline{\Delta f} = \frac{\bar{\delta}}{\pi}, \tag{A11}$$

$$\bar{\delta} = \frac{6.91}{T_{60}}, \tag{A12}$$

where $\overline{\Delta f}$ is the average half-power bandwidth of the resonance peak, and $\bar{\delta}$ is the average damping constant of the water tank.

Appendix B: Measurement of sound power level in an anechoic water tank

This part was carried out in an anechoic water tank of dimensions 25 m × 15 m × 10 m. First, the free-field sound power level of the cylindrical shell model was measured, and the results of these measurements (referred to as the "free-field results") were used to check the accuracy of the SFC method. Then, the free-field sound power level of the spherical sound source was measured, which corresponds to RPL$^{\blacktriangle}$ in Eq. (19).

According to the method described in Ref. [30], a measurement system applicable to the cylindrical shell model was established in the anechoic tank (Fig. B1). The upper end of the cylindrical shell model was closely connected to a rotating device by several steel wire ropes. This rotating device had the functions of rotating (precision 0.1°) and lifting (precision 0.01 m), and it could drive the model to rotate through 0°–360° and lower it to any depth in the tank. The cylindrical shell model was placed at mid-depth in the tank (its upper end was 4.75 m away from the water surface) and the depth remained unchanged during the measurements. The hydrophone array consisted of 29 RHS-20 hydrophones arranged as shown in Fig. B1; this arrangement meets the requirements of far-field test conditions. The water temperature was 25 °C.

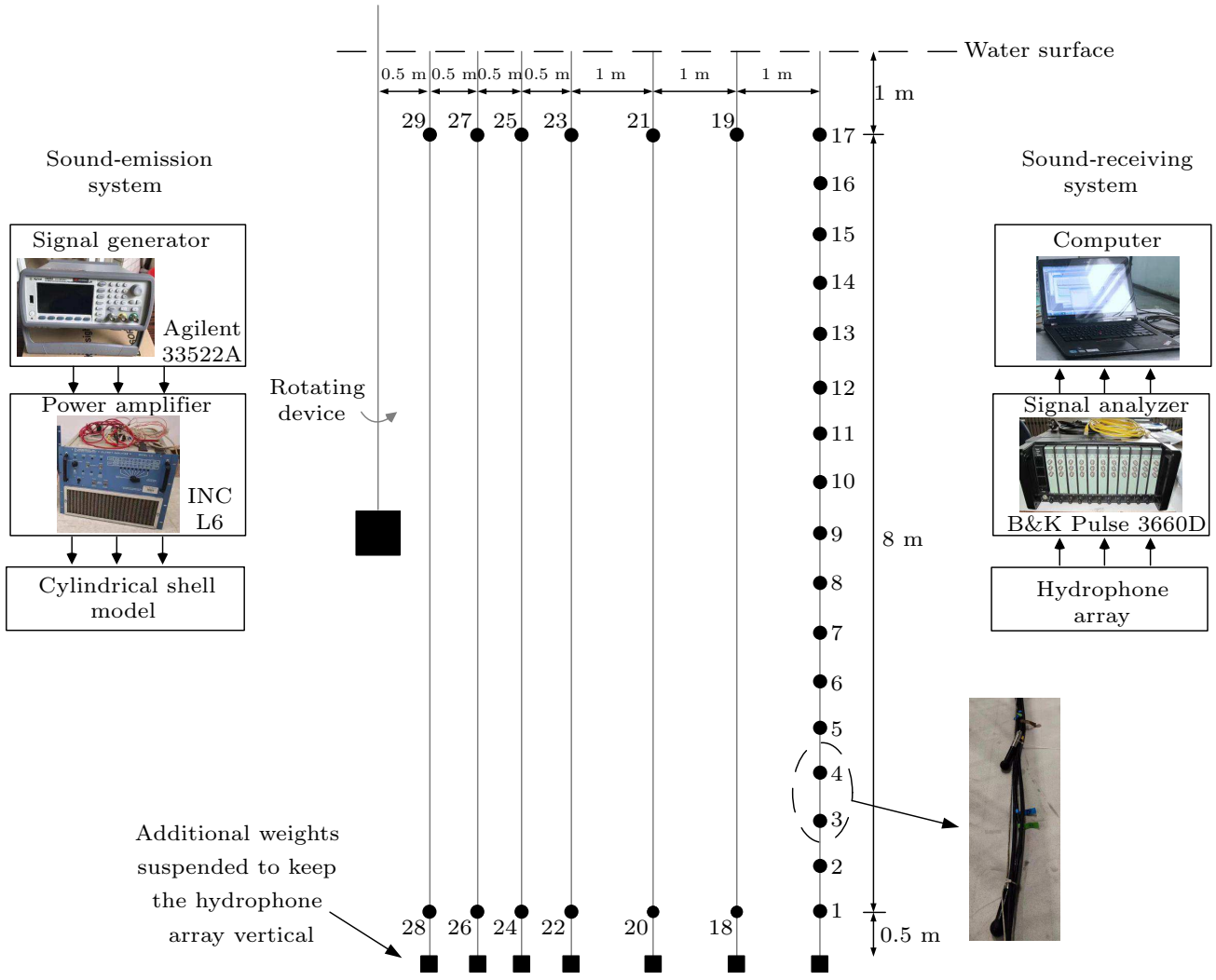
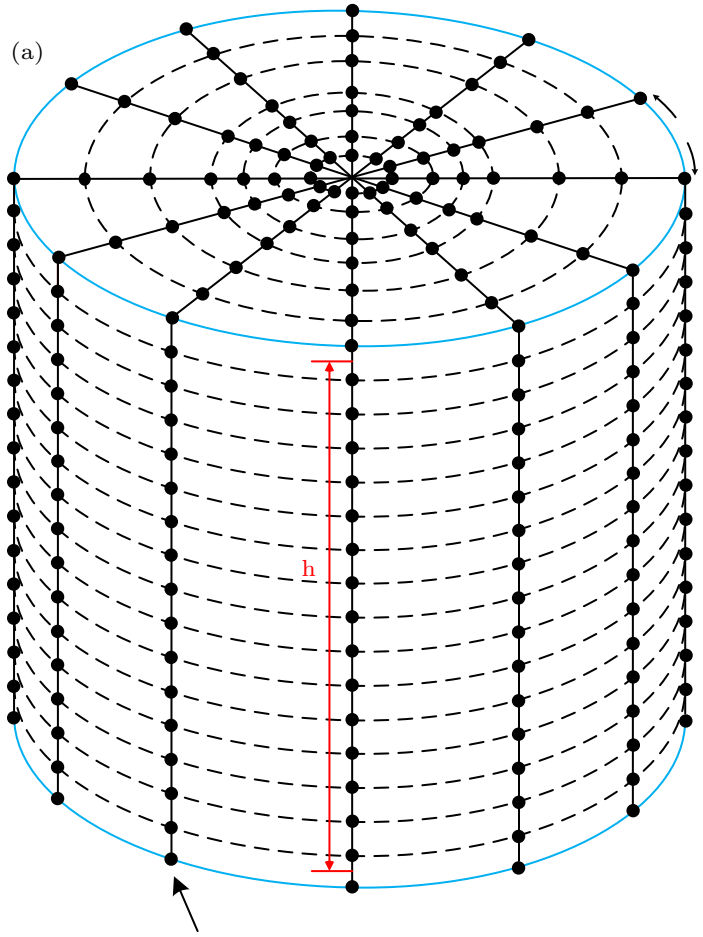


Fig. B1. Measurement system in the anechoic water tank.

The hydrophone array was stationary. In this system, when the rotating device drives the cylindrical shell model to complete a 360° rotation (with rotation angle interval $\Delta\theta$), this is equivalent to the hydrophone array completing a 360° rotation around the stationary model. A cylindrical enclosed measurement surface (with N measurement points) is then formed, as shown in Fig. B2(a). The area of the lateral surface divided by N_3 (i.e., $2\pi R_7 h/N_3$) is equal to the area occupied by each



Number of measurement points on the upper surface: $N_1 = \frac{360^\circ}{\Delta\theta} \times 6$

Number of measurement points at the junction of the upper surface and lateral surface: $N_2 = \frac{360^\circ}{\Delta\theta} \times 1$

Number of measurement points on the lateral surface: $N_3 = \frac{360^\circ}{\Delta\theta} \times 15$

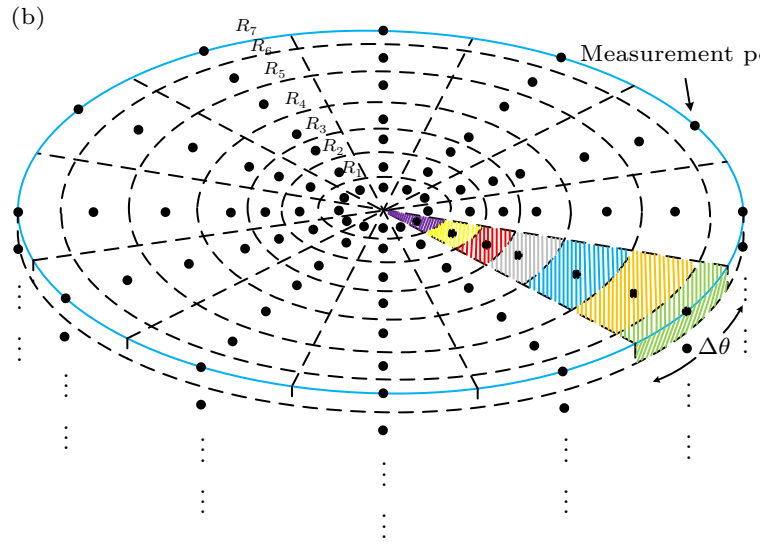
Since the upper and lower surfaces are symmetrical:

Number of measurement points on the lower surface: $N_4 = N_1$

Number of measurement points at the junction of the lower surface and lateral surface: $N_5 = N_2$

$N = N_1 + N_2 + N_3 + N_4 + N_5$

Height of the lateral surface: $h = (0.25 + 14 \times 0.5 + 0.25)$ m



The radii of these circles are:

$R_1 = (0.5 + 0.5/2)$ m $\quad R_2 = (R_1 + 0.5)$ m

$R_3 = (R_2 + 0.5)$ m $\quad R_4 = (R_3 + 0.5/2 + 1/2)$ m

$R_5 = (R_4 + 1)$ m $\quad R_6 = (R_5 + 1)$ m

$R_7 = 5$ m

Area of = $\frac{\pi \times R_1^2}{360^\circ/\Delta\theta}$ m^2

Area of = $\frac{\pi \times (R_2^2 - R_1^2)}{360^\circ/\Delta\theta}$ m^2

Area of = $\frac{\pi \times (R_3^2 - R_2^2)}{360^\circ/\Delta\theta}$ m^2

Area of = $\frac{\pi \times (R_4^2 - R_3^2)}{360^\circ/\Delta\theta}$ m^2

Area of = $\frac{\pi \times (R_5^2 - R_4^2)}{360^\circ/\Delta\theta}$ m^2

Area of = $\frac{\pi \times (R_6^2 - R_5^2)}{360^\circ/\Delta\theta}$ m^2

Area of = $\frac{\pi \times (R_7^2 - R_6^2) + 2 \times \pi \times R_7 \times 0.25}{360^\circ/\Delta\theta}$ m^2

Fig. B2. Diagram of the measurement points (a) on the whole enclosed measurement surface and (b) on the upper surface and at the junction of the upper surface and lateral surface.

measurement point on it. The area occupied by each measurement point on the upper surface and the area occupied by each measurement point at the junction of the upper surface and lateral surface are shown in Fig. B2(b). Since the upper and lower surfaces are symmetrical, the situation of the lower surface will not be repeated here. The sound power level radiated

from the cylindrical shell model in the free-field environment can thus then be expressed as[30]

$$\mathrm{RPL}^{(\mathrm{tv})} = 10\lg\left(\sum_{i=1}^{N}\frac{\bar{P}_i^2}{p_{\mathrm{ref}}^2}S_i\right), \tag{B1}$$

where $\bar{P}_i^2$ denotes the mean-square sound pressure corresponding to the ith measurement point, S_i denotes the area occupied by the ith measurement point, and $p_{\mathrm{ref}} = 1$ μPa is the reference sound pressure.

In the actual measurements, the rotation angle interval $\Delta\theta$ was 10°. A white-noise signal with a bandwidth of 0–3 kHz was generated by the signal generator (33522A, Agilent), and this was amplified by the power amplifier (L6, Instruments, Inc.) and then applied to the longitudinal transducer inside the cylindrical shell model. This enabled the cylindrical shell model to vibrate under the excitation of the transducer. The input amplitude of the signal generator and the gain of the power amplifier were exactly the same as those used in the experiments in the non-anechoic tank (see Subsection 3.2). The acoustic signals collected by the hydrophone array were stored in a computer in the form of the mean-square sound pressure produced by a dynamic analyzer (PULSE 3660D, Brüel & Kjær) for subsequent data processing. Figure B3 shows the measurement results for the free-field sound power level $\mathrm{RPL}^{(\mathrm{tv})}$ of the cylindrical shell model.

Obtaining the sound power radiated from an omnidirectional sound source in a free-field environment is a simple task: it only requires measurement of the sound pressure at any field point in the far-field region and the distance between this field point and the sound source. The measurement system shown in Fig. B1 was nonetheless still used for this, but the power amplifier was replaced with a Brüel & Kjær 2713 because the L6 amplifier could not be used to drive the actuator of the spherical source. During this measurement, the rotating device was used to fix the spherical sound source at 5 m underwater, and a white-noise signal with a bandwidth of 0–3 kHz was generated by the signal generator and amplified by the power amplifier; this was then applied to the spherical sound source to make it emit stably. The input amplitude of the signal generator and the gain of the power amplifier were exactly the same as those used in the experiments in the non-anechoic tank (see Subsection 3.1). It can be seen from Fig. B1 that the No. 9 hydrophone and the spherical sound source were located at the same depth, and the distance between them was 5 m. According to the spherical propagation law, the sound pressure $p_{1\mathrm{f}}$ at a distance of 1 m from the sound source can be calculated using the sound pressure at the No. 9 hydrophone. The free-field sound power level of the spherical sound source can then be obtained as in Ref. [31]:

$$\mathrm{RPL}^{\blacktriangle} = 10\lg\left(\frac{p_{1\mathrm{f}}^2}{p_{\mathrm{ref}}^2}\right) - 10\lg(W_{\mathrm{ref}}) - 170.77. \tag{B2}$$

The measurement results of $\mathrm{RPL}^{\blacktriangle}$ are shown in Fig. B3.

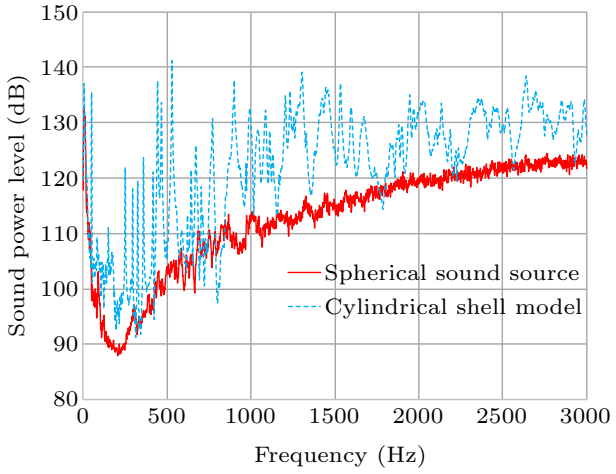


Fig. B3. Measurement results for the free-field sound power levels of the cylindrical shell model and the spherical sound source.

Appendix C: Measurement results corresponding to an excitation force pointing in the +*y* direction

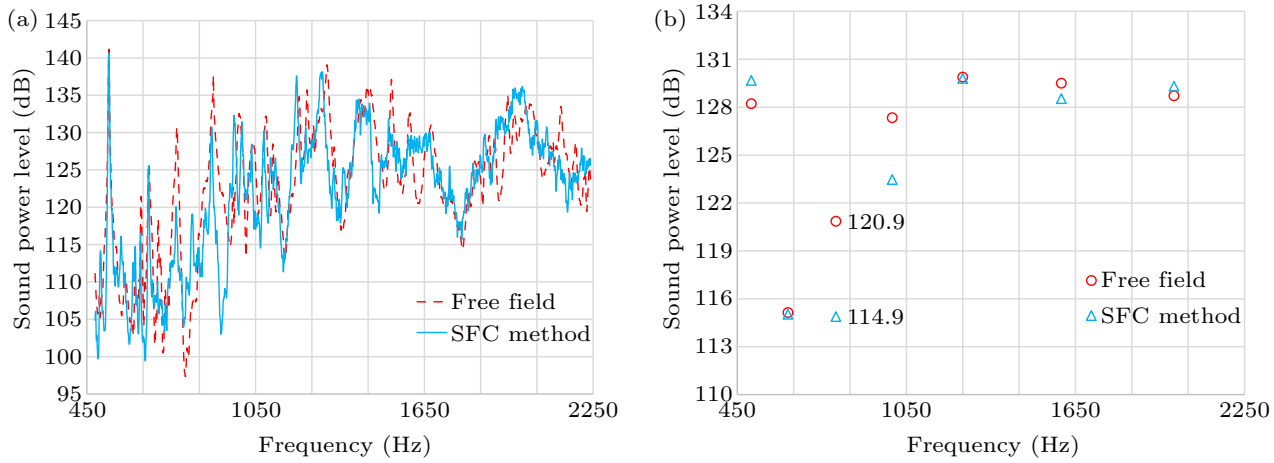


Fig. C1. Measurement results for the sound power level of the cylindrical shell model when emitting at position 5 (with $\boldsymbol{F}_y$ as the direction of the excitation force) (a) in narrow bands and (b) in 1/3-octave bands.

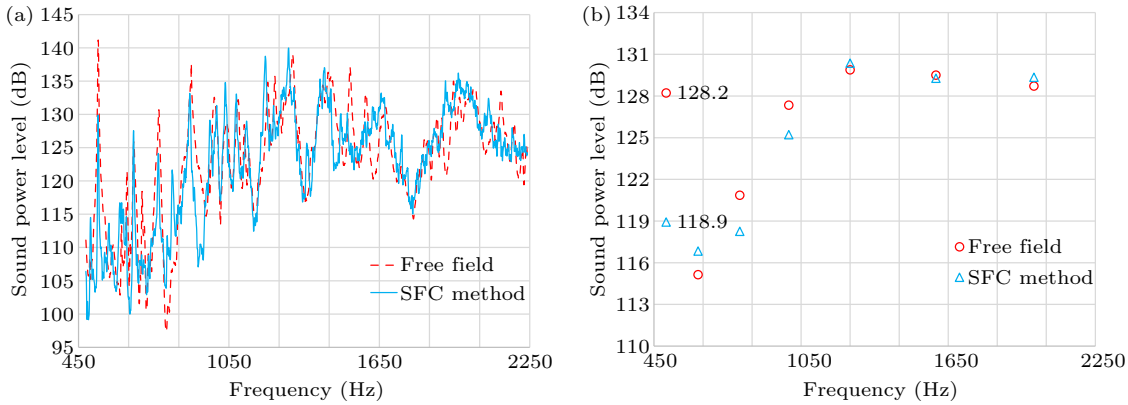


Fig. C2. Measurement results for the sound power level of the cylindrical shell model when emitting at position 6 (with $\boldsymbol{F}_y$ as the direction of the excitation force) (a) in narrow bands and (b) in 1/3-octave bands.

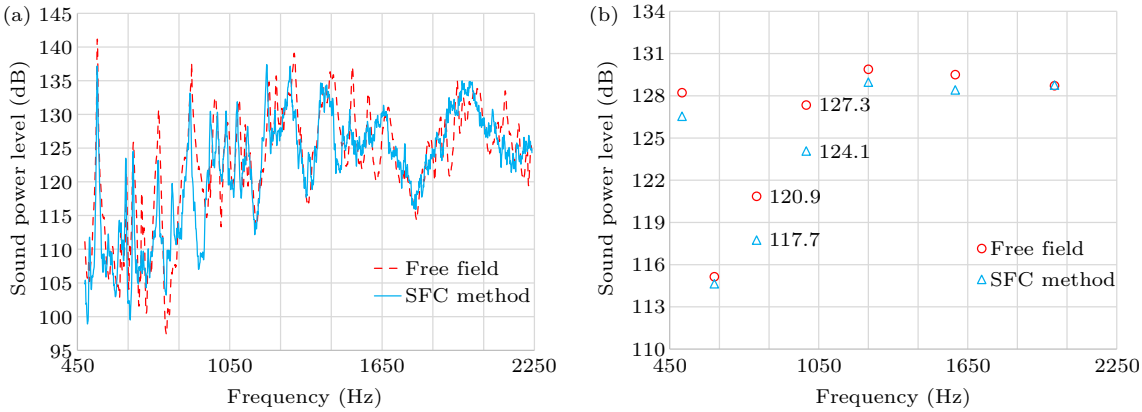


Fig. C3. Measurement results for the sound power level of the cylindrical shell model when four different emission positions were used (positions 5–8, with $\boldsymbol{F}_y$ as the direction of the excitation force) (a) in narrow bands and (b) in 1/3-octave bands.

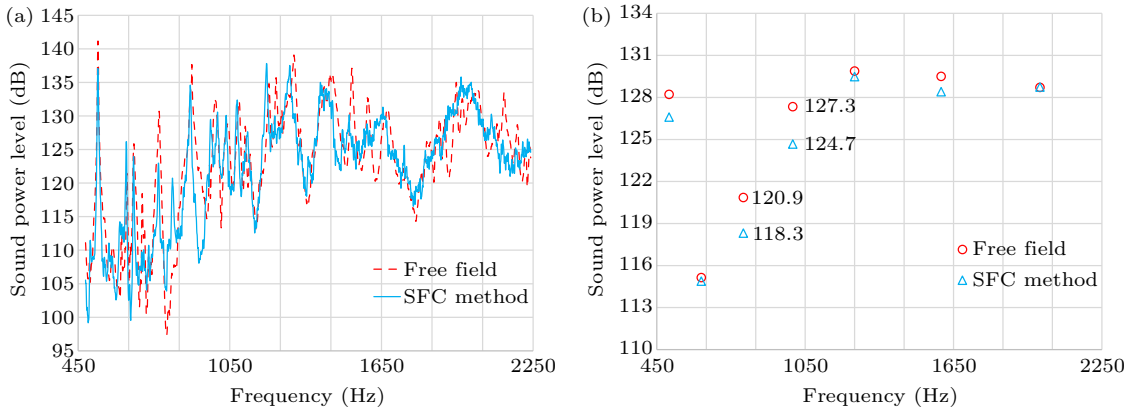


Fig. C4. Measurement results for the sound power level of the cylindrical shell model when seven different emission positions were used (positions 2–8, with $\boldsymbol{F}_y$ as the direction of the excitation force) (a) in narrow bands and (b) in 1/3-octave bands.

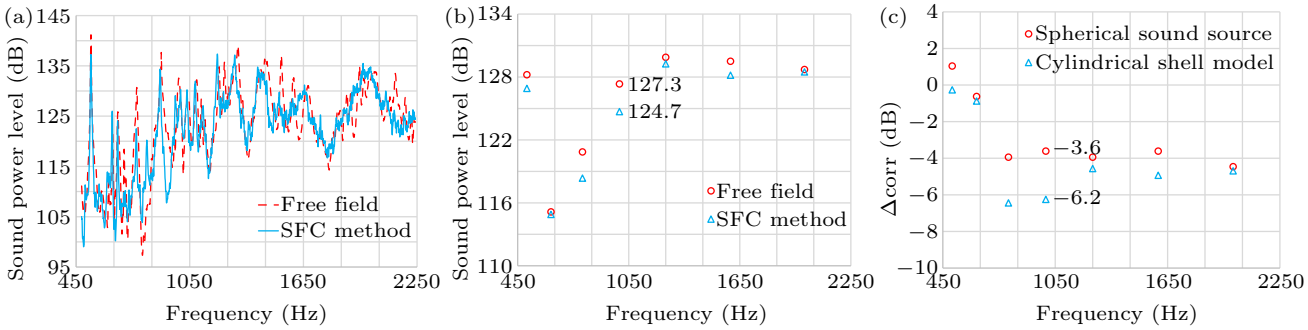


Fig. C5. Measurement results when using eight different emission positions (positions 1–8) for the cylindrical shell model (with $\boldsymbol{F}_y$ as the direction of the excitation force): (a) sound power levels of the model in narrow bands and (b) in 1/3-octave bands, and (c) 1/3-octave spectrum of Δcorr.

Acknowledgments

Project supported by the National Natural Science Foundation of China (Grant No. 11874131) and Open Fund Project of Key Laboratory of Underwater Acoustic Countermeasures Technology (Grant No. 2021-JCJQ-LB033-05).

References

[1] Pangerc T, Theobald P D, Wang L S, Robinson S P and Lepper P A 2016 *J. Acoust. Soc. Am.* **140** 2913
[2] Gassmann M, Wiggins S M and Hildebrand J A 2017 *J. Acoust. Soc. Am.* **142** 1563
[3] Samchenko A N, Kosheleva A V, Shvyrev A N and Pivovarov A A 2014 *Chin. Phys. Lett.* **31** 124301
[4] Jiang G Y, Sun C, Xie L and Liu X H 2019 *Acta Phys. Sin.* **68** 024302 (in Chinese)
[5] Blake W K and Maga L J 1975 *J. Acoust. Soc. Am.* **57** 380
[6] Chen Y, Yang L Q, Zhou L S, Jin X F and Jia G H 2020 *Meas. Sci. Technol.* **32** 035012
[7] Robinson S P, Hayman G, Harris P and Beamiss G 2018 *Meas. Sci. Technol.* **29** 085001
[8] Isaev A E, Matveev A N, Nekrich G S and Polikarpov A M 2014 *Acoust. Phys.* **60** 45
[9] Roux L, Pouille M, Audoly C and Hladky A 2020 *J. Acoust. Soc. Am.* **147** 1104
[10] Li J L, Ma X C, Li S X and Xiao F 2017 *J. Acoust. Soc. Am.* **142** EL478
[11] Kim K 2019 *J. Ocean. Eng. Technol.* **33** 358
[12] Shang D J, Li Q, Shang D J and Lin H 2012 *Acta Acustica* **37** 416
[13] Goldschmidt M Z, Horn J F, Jonson M L and Medvitz R 2021 *IEEE J. Ocean. Eng.* **46** 736
[14] Fischer J, Doolan C, Rowan M, Lamos D, Seers J, Vargas O, Lam S and Skvortsov A 2021 *Appl. Acoust.* **174** 107798
[15] Li Q, Xu H Z, Tang R and Shang D J 2020 *J. Sound Vib.* **489** 115645
[16] Zhang C, Li S H, Shang D J, Han Y Y and Shang Y Y 2020 *Appl. Sci.* **10** 3073
[17] Barnard A R, Hambric S A and Maynard J D 2012 *J. Sound Vib.* **331** 3931
[18] Zhang Y M, Tang R, Li Q and Shang D J 2018 *Meas. Sci. Technol.* **29** 035101
[19] Van de Loock J, Décultot D, Léon F, Chati F, Maze G, Rajaona D R and Klauson A 2013 *J. Acoust. Soc. Am.* **133** EL26
[20] Xu W W, Lai Z N, Wu D Z and Wang L Q 2013 *Appl. Acoust.* **74** 845
[21] Li Q, Song J P, Shang D J and Tang R 2021 *Appl. Acoust.* **182** 108227
[22] Morse P M and Ingard K U 1967 *Theoretical Acoustics* (New York: McGraw-Hill Inc.) pp. 554–599
[23] Kuttruff H 2009 *Room Acoustics* (5th edn.) (Abingdon: Spon Press) pp. 70–71
[24] Smith W F and Bailey J R 1973 *J. Acoust. Soc. Am.* **54** 950
[25] Zhang H L 2012 *Theoretical Acoustics* (Beijing: Higher Education Press) pp. 235–237 (in Chinese)
[26] Li Q, Xie D D, Tang R, Shang D J and Lv Z C 2022 *Chin. Phys. B* **31** 064302
[27] Shang D J, Li Q, Shang D J and Hou B L 2010 *J. Harbin Eng. Univ.* **31** 938 (in Chinese)
[28] Ma D Y 2004 *Fundamentals of Modern Acoustic Theory* (Beijing: Science Press) pp. 171–173 (in Chinese)
[29] Shang D J, Tang R, Li Q and Song J P 2020 *J. Sound Vib.* **468** 115071
[30] Gao Y, Li B and Dai J 2010 *J. Ship Mech.* **14** 1189 (in Chinese)
[31] Urick R J 1983 *Principles of Underwater Sound* (3rd edn.) (New York: McGraw-Hill Inc.) pp. 17–30